Cryoatomic Force Microscopy of Filamentous Actin

Zhifeng Shao,*† Dan Shi,* and Avril V. Somlyo*
*Department of Molecular Physiology and Biological Physics, Health Sciences Center, and †Department of Physics, University of Virginia, Charlottesville, Virginia 22908-0011 USA

ABSTRACT Cryoatomic force microscopy (cryo-AFM) was used to image phalloidin-stabilized actin filaments adsorbed to mica. The single filaments are clearly shown to be right-handed helical structures with a periodicity of ~38 nm. Even at a moderate concentration (~10 μg/ml), narrow, branched rafts of actin filaments and larger aggregates have been observed. The resolution achieved is sufficient to resolve actin monomers within the filaments. A closer examination of the images shows that the branched rafts are composed of up to three individual filaments with a highly regular lateral registration with a fixed axial shift of ~13 nm. The implications of these higher-order structures are discussed in terms of x-ray fiber diffraction and rheology of actin gels. The cryo-AFM images also indicate that the recently proposed model of left-handed F-actin is likely to be an artifact of preparation and/or low-resolution AFM imaging.

INTRODUCTION

Actin is a highly conserved ubiquitous protein expressed in most living organisms, and is a major component of the cytoskeleton (Pollard and Cooper, 1986). Actin in its globular form can be polymerized into long right-handed helical filaments induced by Mg^{2+}, K^+, and Na^+ (Estes et al., 1992; Sheterline et al., 1995). Such filaments can interact with an array of cytoplasmic proteins (Furukawa and Fechheimer, 1997). Not only is actin an essential component in myosin-based motility (Holmes, 1998; Huxley, 1969; Huxley and Simmons, 1971; Pollard, 1990; Bray, 1992), but is also a major structural component (Coluccio and Bretscher, 1989). In addition, actin alone can also mediate motility through controlled polymerization (Smith, 1988) or through gel-sol transitions (Kane, 1975; Pollard et al., 1982). Due to its diverse and critical function in all eukaryotes, the structure of actin has been a major subject of research since its discovery. Not only has the atomic structure of the monomeric G actin been solved in more than one crystal form (Kabsch et al., 1990; McLaughlin et al., 1993; Schutt et al., 1993), but atomic models of the filamentous structure has also been proposed based on fiber x-ray diffraction (Holmes et al., 1990; Lorenz et al., 1993) and electron microscopy (Bremer et al., 1991, 1994; Milligan et al., 1990; Moore et al., 1970). Such structural elucidation has played a pivotal role in our understanding of the function of actin under various conditions.

However, relatively little attention has been given to the structure of higher-order aggregates of F-actin (Aebi et al., 1981; Hanson, 1968; Steinmetz et al., 1998; Sukow and DeRosier, 1998; Suzuki et al., 1989). Actin bundles found in cells such as in the microvilli (Coluccio and Bretscher, 1989) or stress fibers (Byers and Fujiwara, 1982), have generally been associated with actin cross-linking proteins (Furukawa and Fechheimer, 1997), although it is also well established that F-actin can self-associate to form gels in the absence of any actin-binding proteins (Janmey et al., 1994; Zaner, 1995). Such interaction is supported by the polymorphism of actin, which can form various large-scale structures, from bundles to paracrystals to crystalline sheets (Aebi et al., 1981; Kawamura and Maruyama, 1970; O'Brien et al., 1971; Millonig et al., 1988; Taylor and Taylor, 1992). Since F-actin aggregates may also form in cells in conjunction with actin binding proteins, the mechanical, i.e., viscoelastic, properties of polymerized actin have been examined both experimentally and theoretically (Janmey et al., 1994; Zaner, 1995). So far, the structure of these aggregates has not been examined in sufficient detail to permit interpretation of these measurements (Käs et al., 1996).

Finally, a recent AFM study of dehydrated F-actin suggested that the filament could be either left-handed or right-handed (Chang et al., 1995; Bustamante et al., 1994), even though left-handed helical actin filaments have never been observed with other techniques. If such left-handed helical F-actin indeed exists, many of the fundamental issues regarding the mechanism of actin-related function may have to be reexamined. However, the validity of this intriguing claim is open to question, as the diameter of F-actin measured in this study was >20 nm, and the left-handed helical appearance was only apparent after image restoration (Chang et al., 1995; Bustamante et al., 1994). Therefore, before its acceptance, a critical reexamination of this issue seems advisable.

In this paper we report the first cryoatomic force microscopy (cryo-AFM) study of actin filaments. Owing to the improved specimen stability and molecular rigidity in the cryo-AFM, high-resolution images of F-actin have been obtained. This was achieved without resorting to the use of metal shadows (Tyler and Branton, 1980) or image restoration (Keller and Franke, 1993). In these images, single

Received for publication 14 July 1999 and in final form 17 November 1999.
Address reprint requests to Zhifeng Shao, Dept. of Molecular Physiology and Biological Physics, University of Virginia Health Sciences Center, P.O. Box 10011, Charlottesville, VA 22908-0011. Tel.: 804-982-0829; Fax: 804-982-1616; E-mail: zs9q@virginia.edu.

0006-3495/00/02/950/09 $2.00

filaments can be clearly distinguished from multifilament aggregates (branched rafts and meshes), and structures corresponding to two actin monomers within the filaments are directly resolved. Most interesting is the observation that within the observed rafts, neighboring filaments are always registered with the same axial shift and, subsequently, the rafts retain the same axial periodicity as single filaments. Our results further show that the so-called left-handed single actin filaments may be due to the aligned broken fragments, which could not be clearly resolved at low resolution.

MATERIALS AND METHODS

Protein purification

G-actin was purified from rabbit skeletal muscle following the method of Spudich and Watt (1971) and polymerized in the presence of 100 mM KCl, 2 mM $MgCl_2$, and 1 mM ATP. Polymerized actin was stored in a buffer containing 4 mM imidazole, 100 mM KCl, 2 mM $MgCl_2$, 0.5 mM ATP, and 1 mM DTT at 4°C. On SDS-PAGE a single band was observed with no evidence of contamination by other (e.g., actin binding) proteins.

Specimen preparation

Before each experiment particles were removed from all freshly prepared buffers by passing through 0.22-μm filters. To stabilize the actin filaments 1.33 μM TRITC phalloidin was added to the stock actin solution to give a final concentration of actin at 10 μg/ml with a molar ratio of actin to phalloidin at ~1:5. A small volume of the solution, ~2 μl, was then placed on the surface of freshly cleaved mica under clean dry nitrogen and incubated for 15 min at room temperature. The sample was then flushed with 1 ml of solution containing 250 mM ammonium acetate at pH 7.2. A stream of clean nitrogen gas was used to rapidly remove any excess solution remaining on the surface of mica. The specimen was then lowered into the cryo-AFM, which was close to liquid nitrogen temperature. After temperature equilibration the specimen was ready for imaging. For those controls where chemical fixation was applied, the sample was first rinsed with the same buffer, followed by 0.05% glutaraldehyde for 5 s in the same buffer solution. The sample was then flushed with 250 mM ammonium acetate before the last step.

Cryo-AFM imaging

Details of design of the cryo-AFM and its principle of operation have been published elsewhere (Mou et al., 1993; Han et al., 1995). The imaging temperature was maintained at 80–85 K, at a stability of better than 4 mK/min. The long-term drift was <2°C per 12 h period. The change in the piezo scanner sensitivity corresponding to 1°C change is ~1.1% of the full scale. Therefore, over the 30-min period of data collection, image distortion due to temperature drift should be <0.001% (0.1 nm per 10 μm). The bare silicon nitride cantilevers with oxide-sharpened tips were purchased from Park Scientific (Sunnyville, CA). At room temperature, the nominal spring constant was 0.03 nN/nm (~15% greater at 100 K). The adhesion force was kept below 2 nN, and the frame rate (512 × 512 pixels) was from 5 to 50 min. A two-dimensional 1-μm period dot matrix calibration grid provided by Digital Instruments (Santa Barbara, CA) was used to calibrate the AFM piezo scanner. The periodicity of the actin filament also served as an internal calibration of the piezo scanner.

Dimensional measurements

AFM images were first flattened off-line to remove the background slope and the slow drift in the z axis of the piezo scanner. The banding fluctuations, due to laser noise, were also removed with the matching of the base line for each horizontal scan with off-line calculations. Length, full-width at half-height, and height measurements were performed with the use of sectional profiles, available from the software of the NanoScope IIIa (Digital Instruments, Santa Barbara, CA). To reduce random errors the images were zoomed up for dimensional measurements of small features, such as the diameter of the single filaments or the size of the subunits.

RESULTS

Large-scale structures

Highly reproducible images of F-actin were obtained with the cryo-AFM under several slightly different conditions. Two representative images are shown in Fig. 1, *A* and *B*. F-actin is seen to form extensive mesh-like networks in the absence of actin cross-linking proteins and at this relatively low concentration of ~10 μg/ml. In addition to filaments simply crossing over each other, single filaments are seen to branch out from one raft and to join another raft (Fig. 1, *B* and *C*). The branches observed in these studies are very different from the branch-like junctions recently reported (Mullins et al., 1998), in which an actin-binding protein, Arp2/3, was responsible for initiating a branch from an existing filament. With Arp2/3, the branched F-actin was consistently at an angle of attachment of ~70° and, at the junction of the branch, electron microscopy showed an additional mass attributed to Arp2/3. In the cryo-AFM images, however, the angle of attachment ranged between 17° and 86°, which is apparently not specific. Furthermore, no additional mass was ever detected at the branching point even with higher resolution scans. Therefore, these branches are a continuation of existing actin filaments within the rafts rather than an out growth of a new F-actin filament (Fig. 1, *B* and *C*).

Branched F-actin rafts

The most interesting feature of these images is the presence of apparent multifilament aggregates with a well-defined periodicity (see Table 1). Two different types of aggregates may be distinguished in these images upon close examination. The first have a very regular arrangement and contain two or three single filaments (Fig. 2, *A* and *B*). At first glance, these aggregates have the appearance of an intertwined (or twisted) rope of several single actin filaments. However, except in a few cases where the filaments are seen to intertwine with the height of cross-overs corresponding to the number of filaments in the raft, the height of most aggregates is essentially the same as that of a single filament, 5–7 nm. Therefore, we conclude that most of the aggregates are parallel aligned single filaments, similar to the actin rafts described before (see Fig. 2 *C* for a stereograph of a three-filament raft). Interestingly, in such well-formed rafts (we use the word "raft" to describe such highly regular aggregates of F-actin), the neighboring filaments are

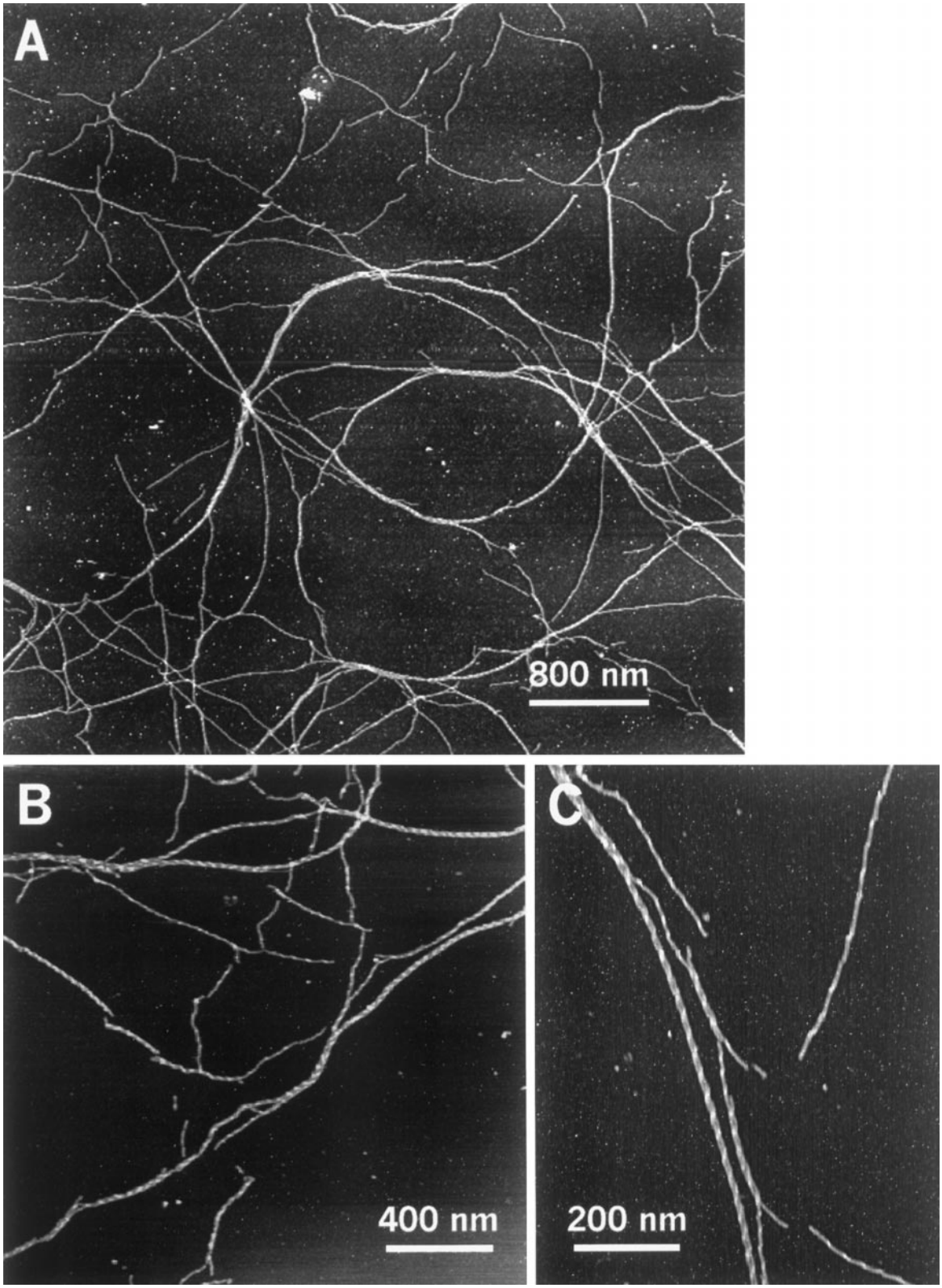

FIGURE 1 Large-scale cryo-AFM image of actin filaments. (A) Both single actin filaments and aggregates are seen over large scales. As shown here, the specimen prepared by this technique is very clean. Except for small aggregates, perhaps of dissociated G-actin, no extensive contamination or aggregation was found. (*B*) At a slightly smaller scale, more details of the actin network are resolved. At this resolution the typical repeat of 37–40 nm is already apparent, although many of the "filaments" have more than one single filament. (*C*) It is clearly shown in this image that single F-actin often branches out from one raft and joins another.

TABLE 1 Full width at half height and periodicity of F-actin filaments

Number of Filaments	Full Width at Half Height (nm)	Periodicity (nm)
1	9 ± 1 (n = 156)	38 ± 3 (n = 81)
2	16 ± 2 (n = 108)	37 ± 2 (n = 95)
3	23 ± 2 (n = 93)	37 ± 2 (n = 97)

registered by an axial shift of 13 ± 2 nm (n = 105). Such registration also seems to further stabilize the regularity of the single filament with a reduced variation in the helical repeat (2 nm vs. 3 nm std.; Table 1). These rafts have a different arrangement than that found with F-actin paracrystals formed on lipid monolayers in the absence of actin cross-linking proteins, where the axial shift between the neighboring filaments is much smaller (Taylor and Taylor, 1992; Ward et al., 1990).

These actin rafts can further aggregate to form more extended ribbonlike structures (Fig. 3). No specific spatial arrangement among the rafts could be identified, and individual actin rafts could be recognized by their defined axial shifts.

To eliminate the possibility that the dehydration process may have produced the highly ordered actin rafts, chemical fixation with glutaraldehyde before dehydration was performed. Similar structures were observed in the presence and absence of fixation. Therefore, the dehydration process has little or no effect on the intrinsic structure of the raft itself. We further examined the possibility that phalloidin could have caused the formation of these rafts. Even though the stability of the actin filaments was much lower in the absence of phalloidin, resulting in a much higher fraction of broken filaments (similar to Fig. 4 *B*), the structure of the rafts was essentially unchanged.

Single actin filaments

Many well-preserved single actin filaments were also observed in the cryo-AFM images (Figs. 1, *B* and *C* and 4 *A*). As already established by electron microscopy (Bremer et

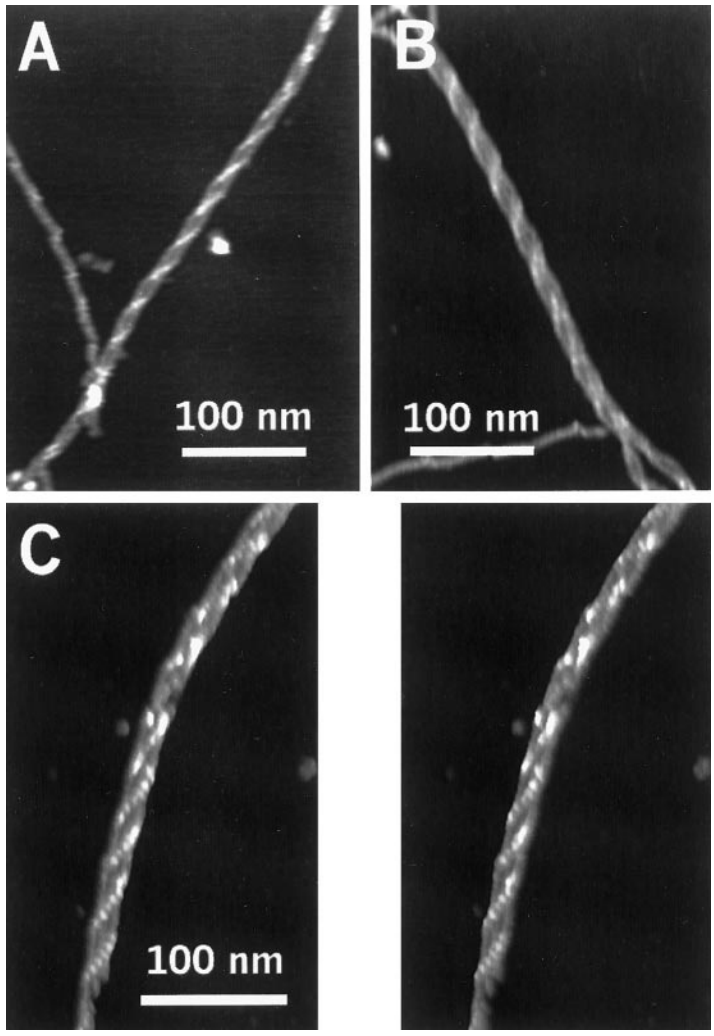

FIGURE 2 Some details of branched F-actin rafts. (*A*) A raft containing two single actin filaments is shown. (*B*) This raft is apparently made of three actin filaments. At the bottom of the image another single filament joins the raft, but the raft itself splits into two rafts with two actin filaments in each. (*C*) A stereograph to show some details of a raft containing three actin filaments. It is noted that within the raft, 5–6 nm modulations are resolved that are due to the actin subunits. In all these actin rafts the regular repeat of F-actin is retained. See text for more details.

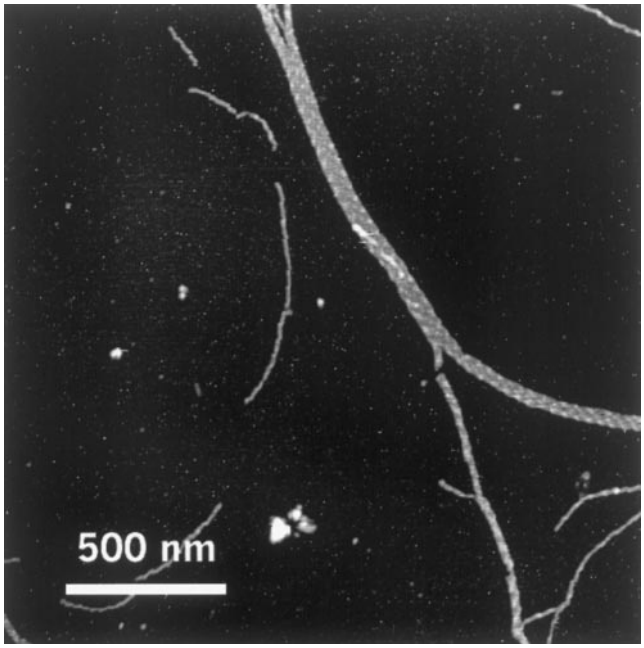

FIGURE 3 F-actin rafts can further associate to form ribbonlike structures, but between the constituting rafts regular registration is not apparent.

al., 1991; Egelman and DeRosier, 1992; Egelman and Orlova, 1995; Fowler and Aebi, 1983), the pitch of the helix of single filaments is variable, with published values around 36 nm. Our measurements give a mean value of 38 ± 3 nm (Table 1), well within the range of more recent electron microscopic studies (Steinmetz et al., 1997) and fiber x-ray diffraction (Holmes et al., 1990). Since the AFM images directly reflect the 3D surface profile of the structure, the right-handed nature of single actin filaments is more than apparent (Fig. 4 *A*, stereograph). However, we also observed that some of the single filaments can form kinks with a periodicity similar to the mean periodicity of well-preserved single filaments. Although a minority within these images, broken fragments of single filaments with segment lengths of 34–42 nm have also been observed (Fig. 4 *B*). Such anomalous structures from the continuous right-handed helix may be attributed to the effect of protein-substrate interaction. During specimen preparation, the interaction between the charged mica surface and F-actin would tend to maximize the contact surface, resulting in the breakage of filaments into fragments of equal length due to their intrinsic helical nature. In this case, the average length of the fragments must be similar to the period of the intact filament. Filaments within the branched rafts do not form such fractured structures, possibly due to the interfilament interaction, which is capable of stabilizing the integrity of each single filament.

The full-width at half-height measured directly from cross-sectional profiles of single filaments is 9 ± 1 nm (n = 156; Table 1). However, the filament center-to-center distance within the rafts, where the effect of the AFM tip is less critical (Shao et al., 1996), is only 7 ± 1 nm (n = 95).

When the specimens were scanned at a smaller scale (i.e., higher spatial resolution), regular modulations along the filament, 6 ± 2 nm, were clearly resolved (Figs. 2 *C* and 4 *C*). The general appearance of the filament surface resembles that of reconstructed surfaces of actin filaments based on electron microscopy (Bremer et al., 1991). Each modulation should contain two actin monomers, but the depression between these two monomers could not be resolved. Based on x-ray fiber diffraction (Holmes et al., 1990), this modulation should be 5.9 nm, in exact agreement with that measured by cryo-AFM.

DISCUSSION

Actin rafts and F-actin structure

The most interesting feature of the actin rafts revealed by cryo-AFM is the highly regular registration between the neighboring filaments (Fig. 2). Such a regular feature strongly suggests the existence of specific contacts between actin filaments. However, at the resolution achieved with the cryo-AFM the orientation of individual filaments in the raft could not be directly determined; but, by using reconstructed F-actin filaments based on electron microscopy (Steinmetz et al., 1997), it is easy to show that both parallel and anti-parallel arrangements could produce a surface feature consistent with that observed by cryo-AFM within the resolution attained while maintaining the 13-nm axial shift between neighboring filaments (Fig. 2). However, since three filament rafts have also been observed and the contacts between the neighboring filaments within the raft must be equivalent, only parallel arrangements can satisfy these conditions. Although the gross features of such a model appear to be consistent with that observed by cryo-AFM, the limited resolution precludes discussion of detailed differences or local structural changes induced by such lateral association. Nevertheless, the 13-nm axial shift clearly distinguishes these structures from those of paracrystals discussed in Steinmetz et al. (1997) or crystalline sheets (Smith et al., 1983).

Actin rafts and fiber x-ray diffraction

Since high-concentration actin solutions (gels) can be aligned through capillary forces (Popp et al., 1987), fiber x-ray diffraction has been used to elucidate the structure of actin filaments (Holmes et al., 1990; Lorenz et al., 1993). However, due to the less ideal alignment of the filaments in the capillary and the lack of a complete data set, the structure had to be based on a self-consistent calculation with built-in parameters to search for a global minimum. So far, such calculations have been performed by making the explicit assumption that only single actin filaments exist in the

capillary. However, since even at the concentration of 10 μg/ml, highly ordered rafts can already form (Figs. 1 and 2), it is probable that actin rafts may also constitute a finite fraction of F-actin in the capillary.

It is straightforward to show that parallel registered rafts do not generate any new layer lines (see Sukow and DeRosier, 1998, for an overview). Therefore, after rotational averaging, the overall diffraction pattern will be qualitatively similar to that generated by single actin filaments. In this case, where the axial shift is $\sim$⅓ of the periodicity of the helix, only higher-order spots show very small differences based on our model calculations. Therefore, even if a large fraction of F-actin in the capillary is in the branched raft form (with two or three actin filaments), the diffraction pattern remains essentially unchanged from that of single filaments within the resolution attainable with fiber diffraction. In fact, the higher-order spots where small differences do exist are normally not detectable in most fiber diffraction patterns. Therefore, it is safe to conclude that fitting such data to a single filament model does not result in detectable deviations (within the resolution limit), and the fitted diameter of the filament, i.e., 9–10 nm (Holmes et al., 1990), should be very close to that of a single filament.

In support of this conclusion, when model filaments with a 9.5-nm maximum diameter, based on fiber x-ray diffraction and electron microscopy, are arranged to have a 13 nm axial shift in a parallel construction and are closely apposite to each other, the center-to-center distance between the filaments turned out to be $\sim$7 nm. This predicted 7 nm center-to-center distance is exactly the value determined by cryo-AFM (7 $\pm$ 1 nm).

Actin rafts and physical measurements

Physical characteristics of F-actin may be influenced by the existence of the branched rafts described in our study. One example is the viscoelasticity of actin gels (Janmey et al., 1990; Zaner, 1995; Zaner and Valberg, 1989). So far, rheological measurements of actin gels have been rather variable (Janmey et al., 1990; Zaner and Valberg, 1989). Although the mechanical property has been attributed to the existence of cross-links between single filaments (Janmey et al., 1990), the nature of such interfilament interactions in pure actin gels has not been elucidated. To explain the response of such gels to shear strain, it was postulated that bundle

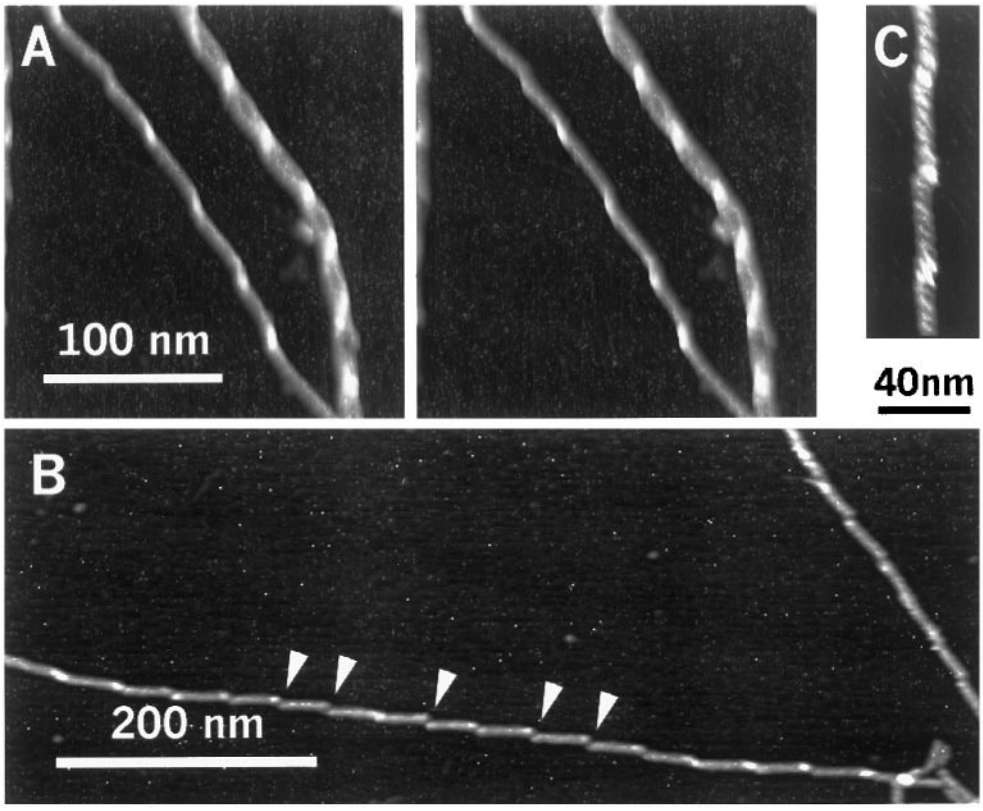

FIGURE 4 Single actin filaments. (*A*) In this stereograph the right-handed nature of F-actin can be seen, although with some distortion. (*B*) From time to time, F-actin filaments are seen to fracture into regular fragments with a length comparable to its regular repeat. The broken points are indicated with arrowheads. This is likely caused by a combination of dehydration and surface interactions (see text for more discussion). (*C*) The regular 5–6 nm modulation in single F-actin is also resolved.

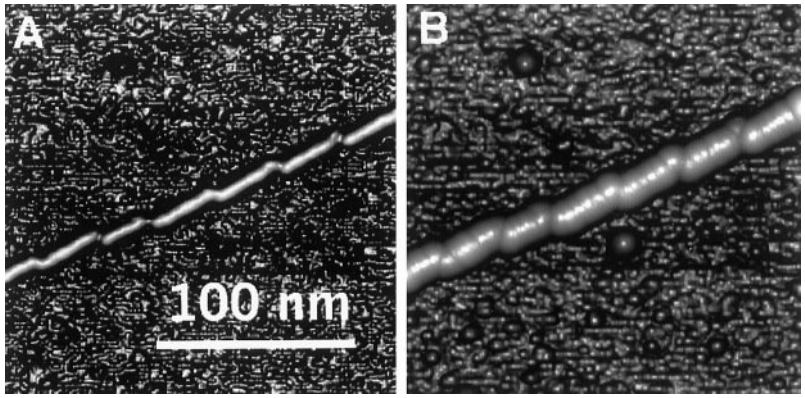

FIGURE 5 Helicity of F-actin. (*A*) Because of the high resolution, the broken points in this F-actin are clearly resolved. Each fragment retains a length similar to the long repeat of the original, right-handed filament. The diameter of the filament is ~10 nm. (*B*) When a hypothetical tip (radius of curvature of 20 nm) is used to dilate the image of (*A*) to produce a lower resolution image, the broken points are no longer as clearly resolved. The diameter of the filament is now ~20 nm. However, since the broken fragments have a slight tilt in respect to the axis of the filament, a left-handed helical impression is thus created. It is noted that this image resembles the restored image presented in Bustamante et al. (1994), including the 5–6 nm modulation along the filament.

formation was an essential aspect of actin network. It was suggested that filaments form islands of concentrated entangled filaments that are connected by "less numerous strands" (Kerst et al., 1990; Cortese and Frieden, 1988). When the applied strain is above a certain threshold, connecting filaments are "disentangled" and shear flow can occur. The observed large-scale structure of F-actin in this work is essentially consistent with the hypothesis of entangled actin filaments (Fig. 1), and may be considered as directly supporting this model. Moreover, low-resolution electron microscopy of actin gels under osmotic stress (Suzuki et al., 1989) also resolved structures similar to those shown in Fig. 1. Therefore, the mesh-like structure where different rafts are "connected" through extensive branching may represent the structural underpinning of the viscoelastic behavior of actin gels. Variations in the preparation of the actin gels may influence the formation of such branched rafts, which may provide an explanation for the somewhat different measurements obtained in different laboratories. Since the "peeling off" of a single filament from a raft may require a minimum amount of force, this could give rise to the observed threshold of shear flow of actin gels.

Helicity of single actin filaments

An intriguing possibility regarding the helicity of F-actin has been raised recently (Chang et al., 1995; Bustamante et al., 1994). In this study, F-actin adsorbed on a mica surface was imaged with AFM in air. Since the width of F-actin measured was ~20 nm, far greater than any known F-actin diameter, the finite size of the tip was considered as the major factor responsible for this low resolution. Even so, after restoration (for a slightly better resolution) (Keller and Franke, 1993), a regular modulation of ~6 nm appeared to be resolvable. Furthermore, the restored filaments had a distinct left-handed hint, although the exact conditions to produce such left-handed helical structures was not defined (Chang et al., 1995; Bustamante et al., 1994). This was, indeed, a novel observation, because neither with electron microscopy nor with fiber x-ray diffraction (Steinmetz et al., 1997; Holmes et al., 1990) have such left-handed structures been found. Therefore, we have carefully examined the cryo-AFM images in an attempt to verify or negate this observation, but found no left-handed helical structures in any of the samples examined, either in single filaments or in the rafts. However, it was more than obvious that actin filaments dried on a mica surface can break into straight segments with a length close to that of the characteristic periodicity (see Fig. 4 *C*). We believe that this is because during the dehydration process the surface tension of the solution tends to flatten the filament to the mica surface, and the electrostatic interaction with mica also tends to maximize the contact area. As a result of these interactions, to maintain its helical topology, the F-actin would first form straight segments connected with sharp kinks at the crossover points. However, when this interaction is beyond a certain threshold, the filaments would break into a series of straight segments, corresponding more or less to the length of the long pitch. Since these straight segments make a tilted angle with the long axis of the filament due to its original helicity, at low resolution, the topology becomes difficult to comprehend, and the filament could appear to have a left-handed helical structure. To illustrate this point, we have calculated the expected AFM image (Fig. 5 *B*) based on the high-resolution cryo-AFM image (Fig. 5 *A*) using a hypothetical tip with a tip radius of curvature of 20 nm. In this calculated image (Fig. 5 *B*), the full-width at half-height is ~20 nm, close to that observed by AFM in air (Chang et al., 1995). Fig. 5 *B* has a very similar appearance to that presented in Bustamante et al. (1994). At this low resolution, the image indeed suggests that the filament might be a left-handed helix. Therefore, we conclude that the so-called left-handed F-actin filaments are simply fractured right-handed filaments, details of which could not be resolved at the low resolution attainable in air, leading to the alternative interpretation of the result.

CONCLUSIONS

Actin filaments adsorbed on mica have been imaged at a resolution sufficient to resolve the characteristic 6 nm mod-

ulation formed by two actin monomers. We show that even at a low actin concentration of 10 μg/ml, F-actin can form complicated, higher-order structures. The most interesting structures found are branched rafts in which up to three single filaments are associated with a highly regular axial registration. Fortunately, such structures only impose a minor effect on the diffraction pattern of aligned F-actin. However, the observed actin rafts may provide a useful structural basis for the understanding of the physical behavior of F-actin. We also conclude that, based on the single filament images, the previously reported left-handed actin filaments based on low-resolution AFM images are likely to be artifacts of specimen preparation.

We thank Justyn Regini for initial data analysis and Yiyi Zhang and Sitong Sheng for technical assistance. We also thank Dr. D. Warshaw for the gift of purified actin, D. Czajkowsky for helpful discussions, and Dr. A. P. Somlyo for a critical reading of the manuscript.

This work was supported by National Institutes of Health Grants RR07720 and HL48807 and a grant from the American Heart Association.

REFERENCES

Aebi, U., W. Fowler, G. Isenberg, T. Pollard, and P. Smith. 1981. Crystalline actin sheets: their structure and polymorphism. *J. Cell Biol.* 91:340–351.

Bray, D. 1992. Cell Movements. Garland Publishing, New York.

Bremer, A., C. Henn, K. N. Goldie, A. Engel, P. R. Smith, and U. Aebi. 1994. Towards atomic interpretation of F-actin filament three dimensional reconstructions. *J. Mol. Biol.* 242:683–700.

Bremer, A., R. C. Millonig, R. Sutterlin, A. Engel, T. D. Pollard, and U. Aebi. 1991. The structural basis for the intrinsic disorder of actin filament: the lateral slipping model. *J. Cell Biol.* 115:689–703.

Bustamante, C., D. A. Erie, and D. Keller. 1994. Biochemical and structural applications of scanning force microscopy. *Curr. Opin. Struct. Biol.* 4:750–760.

Byers, H. R., and K. Fujiwara. 1982. Stress fibers in cells in situ: immunofluorescence visualization with antiactin, antimyosin, and anti-alpha-actinin. *J. Cell Biol.* 93:804–811.

Chang, L., F. Franke, P. Flicker, and D. Keller. 1995. Left and right topography of F-actin filaments. *Proc. SPIE-Int. Soc. Opt. Eng.* 2040: 223–226.

Coluccio, L. M., and A. Bretscher. 1989. Reassociation of microvillar core proteins: making a microvillar core in vitro. *J. Cell Biol.* 108:495–502.

Cortese, J. D., and C. Frieden. 1988. Microheterogeneity of actin gels formed under controlled linear shear. *J. Cell Biol.* 107:1477–1487.

Egelman, E., and D. DeRosier. 1992. Image analysis shows that variations in actin crossover spacings are random, not compensatory. *Biophys. J.* 63:1299–1305.

Egelman, E., and A. Orlova. 1995. New insights into actin filament dynamics. *Curr. Opin. Struct. Biol.* 5:172–180.

Estes, J., L. Selden, H. Kinosian, and L. Gershman. 1992. Tightly bound divalent cations of actin. *J. Muscle Res. Cell Motil.* 13:272–284.

Fowler, W. E., and U. Aebi. 1983. A consistent picture of the actin filament related to the orientation of the actin molecule. *J. Cell Biol.* 97:264–269.

Furukawa, R., and M. Fechheimer. 1997. The structure, function and assembly of actin filament bundles. *Internat. Rev. Cytol.* 175: 29–90.

Han, W., J. Mou, J. Sheng, J. Yang, and Z. Shao. 1995. Cryoatomic force microscopy: a new approach for biological imaging at high resolution. *Biochemistry.* 34:8215–8220.

Hanson, J. 1968. Symposium on muscle. *In* Symp. Biol. Hungarica 8. E. Ernst and F. B. Straub, editors. Aka Kiado, Budapest. 99–103.

Holmes, K. C. 1998. A molecular model for muscle contraction. *Acta Crystallogr. A.* 54:789–797.

Holmes, K. C., D. Popp, W. Gebhard, and W. Kabsch. 1990. Atomic model of the actin filament. *Nature.* 347:44–49.

Huxley, H. 1969. The mechanism of muscular contraction. *Science.* 164: 1356–1366.

Huxley, A., and R. Simmons. 1971. Proposed mechanism of force generation in striated muscle. *Nature.* 233:533–538.

Janmey, P. A., S. Hvidt, J. Käs, D. Lerche, A. Maggs, E. Sackman, M. Schliwa, and T. P. Stossel. 1994. The mechanical properties of actin gels. Elastic modulus and filament motions. *J. Biol. Chem.* 269: 32503–32513.

Janmey, P. A., S. Hvidt, J. Lamb, and T. Stossel. 1990. Effect of ATP on actin filament stiffness. *Nature.* 345:89–92.

Kabsch, W., H. G. Mannherz, D. Suck, E. F. Pai, and K. C. Holmes. 1990. Atomic structure of the actin:DNase I complex. *Nature.* 347:37–44.

Kane, R. 1975. Preparation and purification of polymerized actin from sea urchin egg extracts. *J. Cell Biol.* 66:305–315.

Käs, J., H. Strey, J. X. Tang, D. Finger, R. Ezzell, E. Sackmann, and P. A. Janmey. 1996. F-actin, a model polymer for semiflexible chains in dilute, semidilute, and liquid crystalline solutions. *Biophys. J.* 70: 609–625.

Kawamura, M., and K. Maruyama. 1970. Electron microscopic particle length of F-actin polymerized in vitro. *J. Biochem.* 67:437–457.

Keller, D., J., and F. S. Franke. 1993. Envelope reconstruction of scanning probe microscope images. *Surf. Sci.* 294:409–419.

Kerst, A., C. Chmielewski, C. Livesay, R. E. Buxbaum, and S. R. Heidemann. 1990. Liquid crystal domains and thixotropy of filamentous actin suspensions. *Proc. Natl. Acad. Sci. USA.* 87:4241–4245.

Lorenz, M., D. Popp, and K. C. Holmes. 1993. Refinement of the F-actin model against x-ray fiber diffraction data by the use of a directed mutation algorithm. *J. Mol. Biol.* 234:826–836.

McLaughlin, P. J., J. T. Gooch, H. G. Mannherz, and A. G. Weeds. 1993. Structure of gelsolin segment 1-actin complex and the mechanism of filament severing. *Nature.* 364:685–692.

Milligan, R. A., M. Whittaker, and D. Safer. 1990. Molecular structure of F-actin and location of surface binding sites. *Nature.* 348:217–221.

Millonig, R., H. Salvo, and U. Aebi. 1988. Probing actin polymerization by intermolecular cross-linking. *J. Cell Biol.* 106:785–796.

Moore, P. B., H. E. Huxley, and D. J. DeRosier. 1970. Three-dimensional reconstruction of F-actin, thin filaments and decorated thin filaments. *J. Mol. Biol.* 50:279–295.

Mou, J., J. Yang, and Z. Shao. 1993. An optical detection low temperature atomic force microscope at ambient pressure for biological research. *Rev. Sci. Instrum.* 64:1483–1488.

Mullins, R. D., J. A. Heuser, and T. D. Pollard. 1998. The interaction of Arp2/3 complex with actin-nucleation, high affinity pointed end capping and formation of branching networks of filaments. *Proc. Natl. Acad. Sci. USA.* 95:6181–6186.

O'Brien, E. J., P. M. Bennett, and J. Hanson. 1971. Optical diffraction studies of myofibrillar structure. *Phil. Trans. R. Soc. Lond. B.* 261: 201–208.

Pollard, T. D. 1990. Actin. *Curr. Opin. Cell Biol.* 2:33–40.

Pollard, T. D., U. Aebi, J. A. Cooper, W. E. Fowler, and P. Tseng. 1982. Actin structure, polymerization, and gelation. *Cold Spring Harbor Symp. Quant. Biol.* 46(Pt 2):513–524.

Pollard, T. D., and J. A. Cooper. 1986. Actin and actin-binding proteins. A critical evaluation of mechanisms and functions. *Annu. Rev. Biochem.* 55:987–1035.

Popp, D., V. V. Lednev, and W. Jahn. 1987. Methods of preparing well-orientated sols of f-actin containing filaments suitable for x-ray diffraction. *J. Mol. Biol.* 197:679–684.

Schutt, C. E., J. C. Myslik, M. D. Rozycki, N. C. W. Goonesekere, and U. Lindberg. 1993. The structure of crystalline profilin-beta-actin. *Nature.* 365:810–816.

Shao, Z., J. Mou, D. Czajkowsky, J. Yang, and J. Y. Yuan. 1996. Biological atomic force microscopy: what is achieved and what is needed. *Adv. Physics.* 45:1–86.

Sheterline, P., J. Clayton, and J. C. Sparrow. 1995. Actin. *In*: Protein Profile, Vol. 2. P. Sheterline, editor. Academic Press, New York.

Smith, S. J. 1988. Neuronal cytomechanics: the actin-based motility of growth cones. *Science.* 242:708–715.

Smith, P. R., W. E. Fowler, T. D. Pollard, and U. Aebi. 1983. Structure of the actin molecule determined from electron micrographs of crystalline actin sheets with a tentative alignment of the molecule in the actin filament. *J. Mol. Biol.* 167:641–640.

Spudich, J. A., and S. Watt. 1971. The regulation of rabbit skeletal muscle contraction. I. Biochemical studies of the interaction of the tropomyosin-troponin complex with actin and the proteolytic fragments of myosin. *J. Biol. Chem.* 167:4866–4871.

Steinmetz, O. M., A. Hoenger, P. Tittmann, K. H. Fuchs, H. Gross, and U. Aebi. 1998. An atomic model of crystalline actin tubes: combining electron microscopy with x-ray crystallography. *J. Mol. Biol.* 278: 703–711.

Steinmetz, O. M., D. Stoffler, A. Hoenger, and U. Aebi. 1997. Actin: from cell biology to atomic detail. *J. Struct. Biol.* 119:295–320.

Sukow, C., and D. DeRosier. 1998. How to analyze electron micrographs of rafts of actin filaments crosslinked by actin-binding proteins. *J. Mol. Biol.* 284:1039–1050.

Suzuki, A., M. Yamazaki, and T. Ito. 1989. Osmoelastic coupling in biological structures: formation of parallel bundles of actin filaments in a crystalline-like structure caused by osmotic stress. *Biochemistry.* 28: 6513–6518.

Taylor, K. A., and D. W. Taylor. 1992. Formation of 2D paracrystals of F-actin on phospholipid layers mixed with quaternary ammonium surfactants. *J. Struct. Biol.* 108:140–147.

Tyler, J. M., and D. Branton. 1980. Rotary shadowing of extended molecules dried from glycerol. *J. Ultrastruct. Res.* 71:95–102.

Ward, R., J. Menetret, F. Pattus, and K. Leonard. 1990. Method for forming two dimensional paracrystals of biological filaments on lipid monolayers. *J. Electron Microsc. Tech.* 14:335–341.

Zaner, K. S. 1995. Physics of actin networks. I. Rheology of semi-dilute F-actin. *Biophys. J.* 68:1019–1026.

Zaner, K. S., and P. A. Valberg. 1989. Viscoelasticity of F-actin measured with magnetic microparticles. *J. Cell Biol.* 109:2233–2243.